Measurement of the Full Distribution of Persistent Current in Normal-Metal Rings

M. A. Castellanos-Beltran,[1,*] D. Q. Ngo,[1] W. E. Shanks,[1,†] A. B. Jayich,[1,‡] and J. G. E. Harris[1,2]

[1]*Department of Physics, Yale University, New Haven, Connecticut 06520, USA*

[2]*Department of Applied Physics, Yale University, New Haven, Connecticut 06520, USA*

(Received 12 November 2012; published 9 April 2013)

We have measured the persistent current in individual normal metal rings over a wide range of magnetic fields. From this data, we extract the first six cumulants of the single-ring persistent current distribution. Our results are consistent with the prediction that this distribution should be nearly Gaussian for diffusive metallic rings. This measurement highlights the sensitivity of persistent current to the mesoscopic fluctuations within a single isolated coherent volume.

DOI: 10.1103/PhysRevLett.110.156801 PACS numbers: 73.23.Ra, 73.20.Fz

One of the fundamental archetypes in mesoscopic physics is a system whose volume is sufficiently small that electrons remain quantum coherent within it, yet sufficiently large and complex that its energy spectrum cannot, in practice, be calculated exactly. Such a coherent volume can be realized in a microfabricated metal device cooled to sufficiently low temperatures. The electronic spectrum of such a device will depend upon the angstrom-scale disorder within the metal, which is beyond the control of most fabrication techniques. As a result, the device's spectrum (and all related physical quantities) will be drawn randomly from an ensemble representing the possible realizations of the disorder within nominally identical (i.e., lithographically identical) devices.

The sample-to-sample fluctuations that result from this randomness are characterized by a distribution function P_x. Here, x represents any physical quantity that depends upon the disorder, for example, the conductance g or the persistent current I. These distributions play an important role in our understanding of how electrons flow through disordered materials, for example, in Anderson localization and the scaling theory of conductance [1–3]. For metallic samples (i.e., with mean conductance $\langle g \rangle \gg 1$ in units of e^2/h) calculations predict that P_g and P_I approach a Gaussian distribution as $\langle g \rangle \to \infty$ [4–9]. Deviations from Gaussianity at finite (but large) $\langle g \rangle$ reflect the approach of Anderson localization and the ''breakdown'' of single-parameter scaling that is due to a finite-sized system's vestigial sensitivity to the particular details of its microscopic disorder [3,4].

Several measurements of P_g have been made in systems with $\langle g \rangle \lesssim 1$, including ballistic semiconductor quantum dots [10–12] and semiconductor wires near the localization threshold [13]. In this regime, experiments have found agreement with theory. However, in metallic samples, experiments to date have largely been confined to measurements of $\langle\langle g^2 \rangle\rangle$, the second cumulant of P_g. These measurements of $\langle\langle g^2 \rangle\rangle$ have found excellent agreement with theory in a broad range of circumstances [14–18]. However, little is known experimentally about mesoscopic fluctuations (of g or any other quantity) in metals beyond the second cumulant [18].

Measuring the full distribution of mesoscopic fluctuations in a metal device is challenging. In part this is because most experiments detect g, and so must attach leads to the device. These leads are much larger than the electrons' phase coherence length L_φ, and so contain a large number of coherent volumes that contribute in some degree [14,19,20] to the measured g. (The contribution from the leads is less important when $g \lesssim 1$, as in Refs. [10–13].) Since the fluctuations of each of these coherent volumes are assumed to be independent, higher cumulants of P_g will tend to be suppressed in such a measurement, with the result that the observed fluctuations will appear more Gaussian than the actual P_g. The impact of the leads can be reduced by measuring P_g in long wires (i.e., much longer than L_φ) but this ensures that the wire itself contains many coherent volumes, with the result that the observed fluctuations will again appear more Gaussian than P_g [18].

However, it is possible to measure the mesoscopic fluctuations of *a single coherent volume* by detecting the persistent current I in an isolated metal ring. This has been challenging in the past owing to the small signals involved [21], but it was recently shown that micromechanical torsional magnetometers can measure persistent current with very high sensitivity and low back-action [22,23]. This technique has been applied primarily to arrays of metal rings, with the result that the first two cumulants $\langle\langle I \rangle\rangle$ and $\langle\langle I^2 \rangle\rangle$ of P_I were measured with high precision over a wide range of parameters [23,24]. However, the sensitivity achieved in Ref. [23] (as well as in other studies of individual metal rings [25,26]) did not allow for measurements of individual rings with adequate signal-to-noise ratio (SNR) to resolve the higher cumulants of P_I.

Here we describe measurements of the persistent current in a large number of individual rings. From these measurements we extract the first six cumulants of P_I, as well as other higher-order statistical properties of the persistent current. This is achieved by improving the SNR of the technique described in Refs. [22,23], and by combining

data from more than 400 effectively independent measurements. We find that our results agree with theoretical predictions to within the sensitivity of the measurements. Specifically, we find that the first six cumulants of P_I are consistent with a Gaussian distribution. The small deviations from Gaussianity that are predicted by theory are too small to be detected in our experiment.

A typical device is shown in Fig. 1. It consists of a single-crystal Si cantilever supporting a single Al ring. The fabrication of these devices has been described previously [22,23]. The rings were fabricated via standard electron-beam lithography and were evaporated from a 99.999% purity Al source onto a Si substrate with a native oxide. In addition to the rings, Al wires and contact pads were co-deposited onto the same wafer to allow for transport characterization of the metal. Details of these transport measurements are given in the Supplemental Material [27]. These measurements show that $L_\varphi > 2\pi r$ (r is the rings' mean radius) for the temperatures at which the persistent current is measured. They also provide the electrons' diffusion coefficient $D = 0.020 \pm 0.0015$ m^2/s.

The procedure for measuring the persistent current (PC) has also been described previously [23]. The cantilever's displacement is monitored by a laser interferometer. The signal from the interferometer is used to drive the cantilever in a phase-locked loop, allowing the cantilever's resonance frequency ω_m to be monitored. In the presence of an applied magnetic field B, the persistent current I circulating in the ring produces a torque on the cantilever. This torque changes ω_m, and I is inferred from this change. Details are given in the Supplemental Material [23,27].

Measurements of the PC were made at temperatures 320 mK $< T <$ 365 mK, and magnetic fields 4 T $< B <$ 9 T (applied at an angle $\alpha = 45°$ relative to the rings' plane). This is well above the critical field of Al, ensuring that the rings are in their normal state. The large B is required to produce a detectable torque. It also simplifies the data analysis, as large B within the metal of the ring strongly suppresses the effect of electron-electron interactions on the PC [24], allowing us to compare our results to independent-electron theory (though we note that for large $\langle g \rangle$ interactions are not predicted to make P_I non-Gaussian [6–8]).

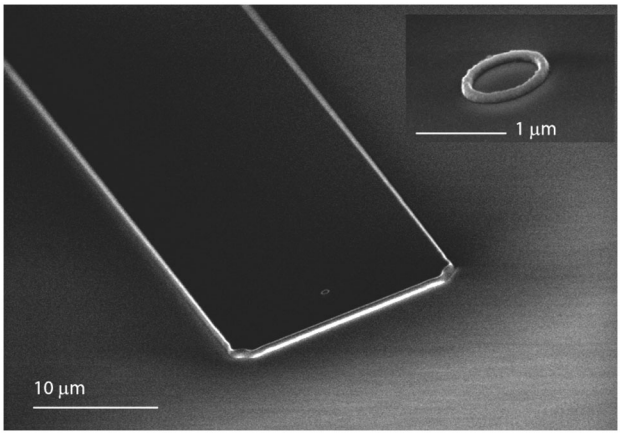

FIG. 1. Scanning electron micrograph of a cantilever with a single ring similar to the ones used in the experiment. Inset: magnified view of the ring. These images show the cantilever and ring prior to their release from the underlying SiO_2 layer.

Measurements were made on eight different rings, with each ring on a separate cantilever. The full data sets from each ring, as well as the rings' dimensions and other properties, are shown in the Supplemental Material [27]. A typical measurement of $I(B)$ for one of these devices (ring #6) is shown in Fig. 2. The rapid oscillations in Figs. 2(a) and 2(b) are due to the Aharonov-Bohm (AB) effect: as B is varied, the magnetic flux $\Phi = BA_\Phi \sin\alpha$ through the ring varies, causing $I(B)$ to oscillate with period $B_{\rm per} = \Phi_0/(A_\Phi \sin\alpha)$. Here $A_\Phi = \pi r^2$ is the typical area enclosed by the electrons in the ring, and $\Phi_0 = h/e$. No higher harmonics of the AB oscillations were observed above the noise floor of the measurement.

The AB oscillations' amplitude (and upon closer inspection, their phase) varies on a field scale larger than $B_{\rm per}$. These aperiodic modulations result from the fact that sweeping B also varies the magnetic flux in the metal of the ring $\Phi_m \approx 2\pi r w B$, where w is the ring's width. Because the ring represents a single coherent volume, its spectrum is expected to be randomized each time Φ_m changes by $\sim\Phi_0$ [28]. The ergodic hypothesis identifies this randomization with a new realization of the

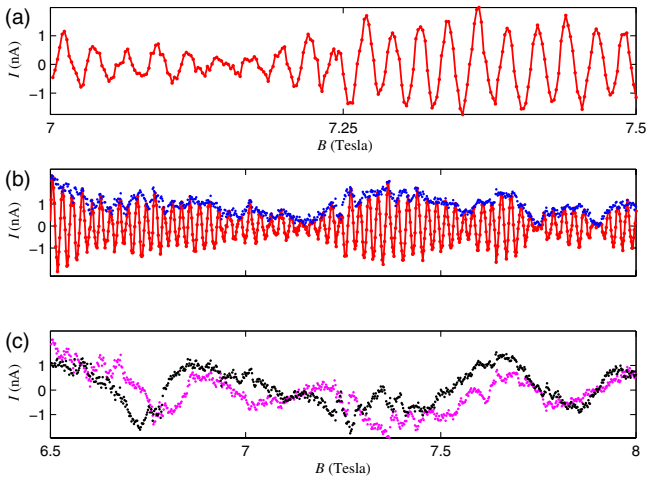

FIG. 2 (color online). Typical measurements of the persistent current in a single ring. (a) A small section of $I(B)$, the persistent current as a function the applied magnetic field. The oscillations are due to the Aharonov-Bohm effect, while the aperiodic modulation arises from flux inside the metal of the ring. (b) Red curve: $I(B)$ over a broader range of magnetic field. Blue curve: the envelope of $I(B)$. (c) The quadrature amplitudes $I^{(+)}$ (black) and $I^{(-)}$ (pink). The envelope in (b) and the quadratures in (c) were extracted by applying the Hilbert transform to the red trace in (b), as described in the Supplemental Material [27].

microscopic disorder [28], so measurements of a single ring over a wide range of B can be interpreted as measurements over a large number of lithographically identical rings. This allows us to use the eight physically distinct rings to measure a much larger number of effectively independent rings. As described below, the large number of effective samples is crucial for making an accurate estimate of the higher cumulants of P_I [29].

Based on these considerations, at large magnetic fields the persistent current is expected to take the form [24]

$$I(\Phi_m, \Phi) = I^{(+)}(\Phi_m)\sin(2\pi\Phi/\Phi_0) + I^{(-)}(\Phi_m)\cos(2\pi\Phi/\Phi_0). \quad (1)$$

Theory makes three predictions concerning $I^{(+)}$ and $I^{(-)}$ (the quadrature amplitudes of the AB oscillations). The first is that they are stochastic functions of Φ_m characterized by a correlation function:

$$\langle I^{(+)}(\Phi_m)I^{(+)}(\Phi_m+\Delta\Phi_m)\rangle = \langle I^{(-)}(\Phi_m)I^{(-)}(\Phi_m+\Delta\Phi_m)\rangle = \langle I^2\rangle C(\Delta\Phi_m/\Phi_c) \quad (2)$$

that decays rapidly for $\Delta\Phi_m \gg \Phi_c$, where Φ_c is the correlation scale, which is typically a few times Φ_0. Both Φ_c and the normalized correlation function $0 \le C(x) \le 1$ have been calculated in Ref. [24].

The second prediction is that the distribution of these quadrature amplitudes $P_{I^{(+)}} = P_{I^{(-)}} = P_I$ is Gaussian in the limit $\langle g\rangle \to \infty$ [6–9]. For finite but large $\langle g\rangle$ it is predicted [6,8,9] that the nth normalized cumulant (defined below) of the persistent current $\kappa_n \sim g^{2-n}$. In our samples $g \sim 10^4$, so these predicted deviations from Gaussianity are well below our present sensitivity (and we note that some κ_n are suppressed still further by a large magnetic field [9]).

Last, correlations between $I^{(+)}$ and $I^{(-)}$ are predicted to be absent [24].

To test these three predictions, we first use the $I(B)$ data from one sample (ring #6, see Supplemental Material [27] for the full data sets and ring parameters) to determine the normalized autocorrelation of the persistent current, $\langle I(B)I(B+\Delta B)\rangle/\langle I^2\rangle$. The result is plotted in Fig. 3, and shows AB oscillations whose envelope initially decays on a field scale that is a few times $\Phi_0/2\pi rw$, in qualitative agreement with the discussion above. After this initial decay the envelope does not approach zero, but instead undergoes apparently random fluctuations. These fluctuations are due to the finite size of the data set, and are discussed below.

We can make a more quantitative comparison with theory by fitting the autocorrelation data in Fig. 3 to the prediction [24] that it should consist of AB oscillations whose envelope is given by $C(\Delta B/B_c)$, where $B_c = \Phi_c/2\pi rw$. The resulting fit is shown as the red line in Fig. 3. The fit parameters are $B_c^{(6)} = 37$ mT and $B_{\rm per}^{(6)} = 25$ mT (where the superscript denotes the ring no.), in good agreement with the dimensions of the ring. The

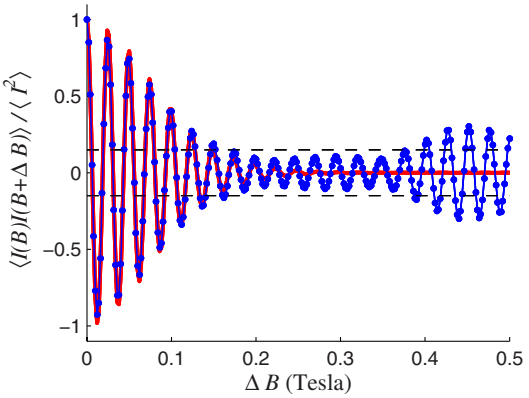

FIG. 3 (color online). Autocorrelation of the persistent current in a single ring. The blue curve is the normalized autocorrelation of the $I(B)$ data from ring #6, while the red curve is a fit to theory. Only data with $\Delta B < 0.3$ was used for the fit. The expected error in the autocorrelation (due to the finite size of the data set) is indicated by the dashed horizontal lines. Similar behavior was observed in all eight rings.

autocorrelation data from the other seven rings showed comparable agreement with the theoretical prediction, although the fitted values of B_c varied from ring to ring (all values of the $B_c^{(i)}$ are given in the Supplemental Material [27]). This analysis provides us with two useful results. The first result is the agreement between the measured and predicted form of $C(x)$, which justifies our use of the analytic expression [24] for $C(x)$ in the analyses below. The second result is the determination of the correlation field $B_c^{(i)}$ for each ring, which will also be used below.

To determine the form of the distribution P_I from our measurements, we begin by applying the Hilbert transform to the $I(B)$ data from each ring. This provides the quadrature amplitudes $I^{(+)}(B)$ and $I^{(-)}(B)$, as shown in Fig. 2(c). It is then straightforward to compute the cumulants of $I^{(+)}$ and $I^{(-)}$, e.g., from their moments. Since there is no physical distinction between $I^{(+)}$ and $I^{(-)}$ when $\Phi_m \gg \Phi_0$, we consider the average of their cumulants: $\langle\langle I^n\rangle\rangle \equiv \frac{1}{2}(\langle\langle (I^{(+)})^n\rangle\rangle + \langle\langle (I^{(-)})^n\rangle\rangle)$. To account for variations between the rings (e.g., of D, r, and T), the contribution to $\langle\langle I^n\rangle\rangle$ from each ring is normalized by the variance $\langle\langle I^2\rangle\rangle$ of that ring, giving the normalized cumulant $\kappa_n \equiv \langle\langle I^n\rangle\rangle/\langle\langle I^2\rangle\rangle^{n/2}$ for the entire data set.

The first several κ_n are plotted as blue circles in Fig. 4(a). The prediction that P_I is Gaussian (corresponding to $\kappa_n = 0$ for all $n \ge 3$) is indicated by the black circles in Fig. 4(a). The data appear qualitatively consistent with a Gaussian distribution; however, to make a meaningful comparison between experiment and theory we estimate the uncertainty in these values. The two most important sources of uncertainty in the measurements of κ_n are the finite SNR of the $I(B)$ data and the finite size of the data set from which the κ_n are calculated. We estimate the impact of the former by applying standard error-propagation

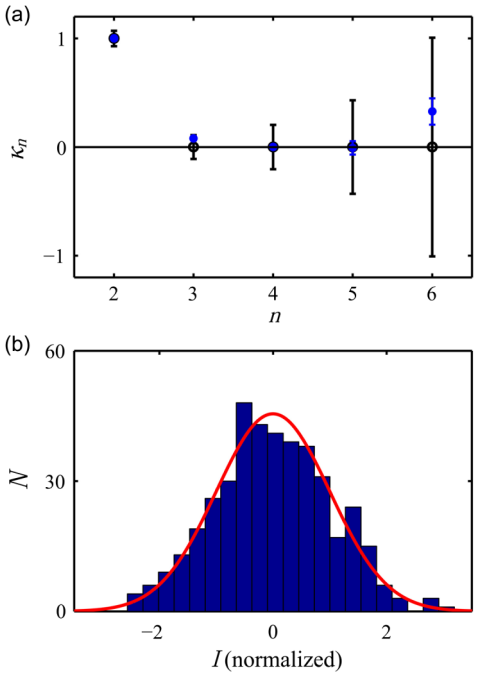

FIG. 4 (color online). The measured distribution of persistent current. (a) Cumulants of the persistent current distribution, calculated from the combined data for all eight rings. Blue circles are the measured cumulants, and black circles are the cumulants expected for a Gaussian distribution. Black error bars: statistical uncertainty from the finite sample size. Blue error bars: statistical uncertainty from the finite signal-to-noise ratio. (b) Histogram of the observed persistent currents. To reduce oversampling artifacts, the data is first binned to give data points that are approximately independent. The solid line is the no-free-parameters prediction.

techniques to the known uncertainty in each $I(B)$ measurement. This procedure is described in the Supplemental Material [27], and leads to the blue error bars in Fig. 4(a).

The finite size of the data set leads to a statistical uncertainty $\delta\kappa_n$ in the estimate of each κ_n. If the data sets for $I^{(+)}(B)$ and $I^{(-)}(B)$ each consisted of uncorrelated data points, then values for the $\delta\kappa_n$ could be found in standard statistics references. However, it is clear from Figs. 2(c) and 3 that each quadrature of the AB oscillations contains correlations that are characterized by the function $C(\Delta B/B_c)$. In this case the $\delta\kappa_n$ depend upon the form of $C(x)$, the value of B_c, and the value of B_{span}, the range of B over which the PC is measured [29],

$$\delta\kappa_n \equiv \langle\kappa_n^2\rangle^{1/2} = \left(n!c_n \frac{B_c}{B_{\text{span}}}\langle\kappa_2\rangle^n\right)^{1/2},$$
$$c_n = \int_{-\infty}^{\infty} (C(x))^n dx \qquad (3)$$

(where the dependence of B_c, B_{span}, and c_n upon the ring no. has been suppressed). The black error bars in Fig. 4(a) correspond to the $\delta\kappa_n$ calculated from Eq. (3). Since $\delta\kappa_n < 1$ only for $n < 7$, we plot the results only up to κ_6.

In addition to calculating the cumulants of P_I from our data, we can also plot the measured P_I in the form of a histogram of the $I^{(+)}(B)$ and $I^{(-)}(B)$ data. To reduce oversampling artifacts in this histogram, we first bin the $I^{(+)}(B)$ and $I^{(-)}(B)$ data into a smaller data set. We choose the size of this smaller data set to correspond to the number of effectively independent data points in the entire data set [29] (i.e., from all eight physically distinct rings): $N_{\text{eff}} = 2\sum_{i=1}^{8} B_{\text{span}}^{(i)}/c_n^{(i)}B_c^{(i)} \approx 412$ (the factor of 2 in this expression arises from the two quadratures). Here we have used $n = 2$ somewhat arbitrarily, but we note that N_{eff} depends only weakly upon the choice of n. As in the calculations of the κ_n, the $I^{(+)}(B)$ and $I^{(-)}(B)$ data from each different ring are normalized by their own variance to account for differences among the rings. The histogram of the resulting data set is shown in Fig. 4(b), along with the no-free-parameter prediction that this histogram should be Gaussian with zero mean and unit variance.

We can use these results to understand the apparently random fluctuations of the autocorrelation data in Fig. 3. At large ΔB, the data are expected to be uncorrelated [i.e., $C(x)$ approaches zero for large x]. However, the standard error of the autocorrelation of a data set consisting of N independent samples is [30] $\delta C = 1/\sqrt{N}$. The data set for ring #6 contains $N_{\text{eff}}^{(6)} = 44$ independent samples; thus at large ΔB the envelope of the autocorrelation in Fig. 3 should have a typical value ≈ 0.15. This value is indicated by the dashed lines in Fig. 3, and is in agreement with the data.

Last, we test our data for correlations between the quadrature amplitudes. From the $I^{(+)}(B)$ and $I^{(-)}(B)$ data it is straightforward to calculate the experimental value of $\rho_{+-} \equiv \text{cov}(I^{(+)}, I^{(-)})/\sqrt{\langle\langle I^{(+)2}\rangle\rangle\langle\langle I^{(-)2}\rangle\rangle}$ which is predicted [24] to be zero. From our data we find $\rho_{+-} = 0.02 \pm 0.05$, where the uncertainty arises from the finite size of the data set. This result is consistent with the prediction that $I^{(+)}(B)$ and $I^{(-)}(B)$ should be independent of each other.

We acknowledge support from the National Science Foundation (NSF) (Grants No. 0706380, No. 0653377, and No. 1106110) and from the US-Israel Binational Science Foundation (BSF). Facilities use was supported by YINQE and NSF MRSEC DMR 1119826. We thank Amnon Aharony, Ora Entin-Wohlman, Leonid Glazman, Rob Ilic, Yoseph Imry, Felix von Oppen, and A. Douglas Stone for their assistance.

*Present address: National Institute for Standards and Technology, Boulder, CO 80305, USA.
†Present address: Department of Electrical Engineering, Princeton University, Princeton, NJ 08544, USA.
‡Present address: Department of Physics, UCSB, Santa Barbara, CA 93106, USA.

[1] P. W. Anderson, Phys. Rev. **109**, 1492 (1958).
[2] E. Abrahams, P. W. Anderson, D. C. Licciardello, and T. V. Ramakrishnan, Phys. Rev. Lett. **42**, 673 (1979).
[3] B. Shapiro, Philos. Mag. B **56**, 1031 (1987).
[4] B. L. Al'tshuler, V. E. Kravtsov, and I. V. Lerner, Sov. Phys. JETP **64**, 1352 (1986).
[5] M. C. W. van Rossum, I. V. Lerner, B. L. Altshuler, and T. M. Nieuwenhuizen, Phys. Rev. B **55**, 4710 (1997).
[6] R. A. Smith and V. Ambegaokar, Europhys. Lett. **20**, 161 (1992).
[7] H. J. Bussemaker and T. R. Kirkpatrick, Phys. Rev. B **56**, 4529 (1997).
[8] M. Houzet, Phys. Rev. B **82**, 161417 (2010).
[9] J. Danon and P. W. Brouwer, Phys. Rev. Lett. **105**, 136803 (2010).
[10] A. M. Chang, H. U. Baranger, L. N. Pfeiffer, K. W. West, and T. Y. Chang, Phys. Rev. Lett. **76**, 1695 (1996).
[11] J. A. Folk, S. R. Patel, S. F. Godijn, A. G. Huibers, S. M. Cronenwett, C. M. Marcus, K. Campman, and A. C. Gossard, Phys. Rev. Lett. **76**, 1699 (1996).
[12] A. G. Huibers, S. R. Patel, C. M. Marcus, P. W. Brouwer, C. I. Duruöz, and J. S. Harris, Jr., Phys. Rev. Lett. **81**, 1917 (1998).
[13] W. Poirier, D. Mailly, and M. Sanquer, Phys. Rev. B **59**, 10856 (1999).
[14] R. A. Webb *et al.*, in *Physics and Technology of Submicron Structures*, edited by H. Heinrich, G. Bauer, and F. Kuchar (Springer-Verlag, Berlin, 1988), p. 98.
[15] A. Benoit *et al.*, in *Anderson Localization*, edited by T. Ando and H. Fukuyama (Springer-Verlag, Berlin, 1988), p. 346.
[16] C. W. J. Beenakker and H. van Houten, Solid State Phys. **44**, 1 (1991).
[17] S. Washburn and R. A. Webb, Rep. Prog. Phys. **55**, 1311 (1992).
[18] V. Fal'ko, I. Lerner, O. Tsyplyatyev, and I. Aleiner, Phys. Rev. Lett. **93**, 159701 (2004).
[19] V. Chandrasekhar, D. E. Prober, and P. Santhanam, Phys. Rev. Lett. **61**, 2253 (1988).
[20] H. U. Baranger, A. D. Stone, and D. P. DiVincenzo, Phys. Rev. B **37**, 6521 (1988).
[21] L. Saminadayar, C. Bauerle, and D. Mailly, Encycl. Nanosci. Nanotech. **3**, 267 (2004).
[22] A. C. Bleszynski-Jayich, W. E. Shanks, B. R. Ilic, and J. G. E. Harris, J. Vac. Sci. Technol. B **26**, 1412 (2008).
[23] A. C. Bleszynski-Jayich, W. E. Shanks, B. Peaudecerf, E. Ginossar, F. von Oppen, L. Glazman, and J. G. E. Harris, Science **326**, 272 (2009).
[24] E. Ginossar, L. I. Glazman, T. Ojanen, F. von Oppen, W. E. Shanks, A. C. Bleszynski-Jayich, and J. G. E. Harris, Phys. Rev. B **81**, 155448 (2010).
[25] V. Chandrasekhar, R. A. Webb, M. J. Brady, M. B. Ketchen, W. J. Gallagher, and A. Kleinsasser, Phys. Rev. Lett. **67**, 3578 (1991).
[26] H. Bluhm, N. C. Koshnick, J. A. Bert, M. E. Huber, and M. A. Moler, Phys. Rev. Lett. **102**, 136802 (2009).
[27] See Supplemental Material at http://link.aps.org/supplemental/10.1103/PhysRevLett.110.156801 for information on the transport characterization of the deposited metal, the data analysis used for the measurement of the persistent current, the parameters of the individual rings, and the complete data set from each ring.
[28] P. A. Lee and A. D. Stone, Phys. Rev. Lett. **55**, 1622 (1985).
[29] O. Tsyplyatyev, I. L. Aleiner, V. I. Falko, and I. V. Lerner, Phys. Rev. B **68**, 121301(R) (2003).
[30] M. G. Kendall and A. Stuart, *The Advanced Theory of Statistics* (Griffin, London 1976), Vol. 1, 4th ed.